Broadband Terahertz Detection With Zero-Bias Field-Effect Transistors Between 100 GHz and 11.8 THz With a Noise Equivalent Power of 250 pW/√Hz at 0.6 THz

Regensburger, S.; Mukherjee, A. K.; Schönhuber, S.; Kainz, M. A.; Winnerl, S.; Klopf, J. M.; Lu, H.; Gossard, A. C.; Unterrainer, K.; Preu, S.;

Originally published:

July 2018

IEEE Transactions on Terahertz Science and Technology 8(2018), 465-471

DOI: https://doi.org/10.1109/TTHZ.2018.2843535

Perma-Link to Publication Repository of HZDR:

https://www.hzdr.de/publications/Publ-27949

Broadband Terahertz Detection with Zero-Bias Field-Effect Transistors between 100 GHz and 11.8 THz with a Noise Equivalent Power of 250 pW/$\sqrt{\text{Hz}}$ at 0.6 THz

Stefan Regensburger, Amlan k. Mukherjee, Sebastian Schönhuber, Martin A. Kainz, Stephan Winnerl, J. Michael Klopf, Hong Lu, Arthur C. Gossard, Karl Unterrainer, and Sascha Preu

***Abstract*—We demonstrate UV contact-lithographically fabricated III-V field effect transistors examined over a bandwidth of 100 GHz to 11.8 THz. The zero-bias device reaches a noise equivalent power as low as 250 pW/$\sqrt{\text{Hz}}$ at 0.6 THz which then increases as f^4 at higher frequencies. The responsivity is modeled by a simple equivalent circuit, showing good agreement over the frequency range of 2 decades. The FETs have been characterized using a photomixer, a quantum cascade laser and a free electron laser, proofing the versatility and large applicability of the detection concept.**

***Index Terms*—Field Effect Transistor, HEMT, Plasma waves, Terahertz (THz), Free Electron Laser, Semiconductor detectors**

I. Introduction

LOW noise Terahertz (100 GHz to 10 THz) detectors are key components of all Terahertz setups and experiments, as the power of inexpensive broadband tabletop THz sources is still low as compared with adjacent parts of the electromagnetic spectrum. At room temperature, coherent detectors offer the lowest noise floor. In homodyne or heterodyne detection mode, field-effect transistors (FETs) have reached noise equivalent powers as low as 8 fW/Hz [1]. Coherent detectors, however, can only be used in systems where phase-locking between source and receiver is possible. Heterodyne detection needs a local oscillator, which can be a technological challenge for ultra broadband detectors. Further, coherent detectors actually detect the THz field instead of THz power. Therefore, their noise equivalent power (NEP) scales as W/Hz while the NEP of square law (i.e. power) detectors scales as W/$\sqrt{\text{Hz}}$. The latter is particularly beneficial for applications that require large IF bandwidths, e.g. in THz communication. To date, the square law detectors with the lowest demonstrated NEP at room temperature are Schottky diodes. Schottky diodes exploit the non-linearity of the IV characteristics to rectify an incoming RF signal. Narrow band designs reach noise equivalent powers (NEPs) of $0.4\,\text{pW}/\sqrt{\text{Hz}}$ [2] in the upper microwave range (88 GHz) and a few pW/$\sqrt{\text{Hz}}$ around 600 GHz [3]–[5]. An important design criterion for Schottky diodes is zero-bias operation in order to circumvent external noise contributions by a biasing circuit and to simplify the setup. Zero-bias Schottky diodes faced a long development, dating back around 50 years, yet with stagnating performance improvement. Within the last years, field-effect transistors (FETs) have become a popular alternative for square law THz detection [6], [7], yet with similar or even shorter response time in the 20 ps range [8]. FETs have become sensitive enough to be used in combination with a quantum cascade laser (QCL) around 3 THz [9]. Rectification in FETs is due to simultaneous modulation of the carrier concentration in the transistor channel, typically a two-dimensional electron gas, by a THz bias, $en^{(2D)} = cU_{\text{THz}}$ and the carrier velocity, $v = \mu E_{\text{THz}} \sim U_{\text{THz}}$, where μ is the carrier mobility and c is the gate-channel capacitance per unit area. The THz bias is often generated by an attached on-chip antenna that receives an incoming THz signal. The output current, $j = env \sim U_{\text{THz}}^2$ contains a rectified DC component simply because the square of the bias is strictly positive. Further details on the rectification effect can be found elsewhere [10], [11]. To date, FET rectifiers reach NEPs in the range of 14 to 20 pW/$\sqrt{\text{Hz}}$ at 720 and 590 GHz [12], [13] with narrow band designs. While this is still higher than the NEPs of Schottky diodes, the NEP of THz-tailored FETs has improved by 4 to 5 orders of magnitude within the last 10 years. A particular

Manuscript received February 23rd, 2018. This work was supported by the Deutsche Forschungsgemeinschaft, Project PR1413/2-1 (LAFET).

S. Regensburger, A. k. Mukherjee, and S. Preu are with Technische Universität Darmstadt, Germany. (e-mail: regensburger@imp.tu-darmstadt.de)

S. Schönhuber, M. A. Kainz, and K. Unterrainer are with TU Wien, Austria.

S. Winnerl, J. M. Klopf are with the Helmholtz Zentrum Dresden-Rossendorf, Germany.

H. Lu is with the University of Nanjing, China.

A. C. Gossard is with the University of California, Santa Barbara, USA.

advantage over Schottky diodes is high reproducibility [14], yet leading to first FET-based camera concepts [15]. Further, Silicon-based and III-V based FETs are compatible with CMOS foundry processes. While in most concepts a (small) gate bias is applied to fine-tune the device responsivity, in this paper we show devices optimized for zero-bias operation in order to minimize external noise. We further demonstrate that the high mobility of III-V FETs allows for much larger structures, relieving limitations by processing technology while still reaching a NEP as low as $250\,\mathrm{pW}/\sqrt{\mathrm{Hz}}$ at 600 GHz with UV contact lithography and an ultra-broadband design. We show good agreement of an equivalent circuit model for FET rectifiers [14], [16] over a frequency range of more than two decades. The devices are characterized using a CW photomixing setup, a QCL [17] and a free electron laser, demonstrating the versatility of FETs different fields of application.

II. Transistor Layout

Fig. 1 (a) shows the high electron mobility (HEMT) structure of the field effect transistors. Two FETs have been fabricated. Both feature a remote doping, yielding a channel electron density of sample A of $4.6{\cdot}10^{11}\,/\mathrm{cm}^2$ at a mobility of $6000\pm100\,\mathrm{cm}^2/\mathrm{Vs}$ and $7.1{\cdot}10^{11}\,/\mathrm{cm}^2$ at a mobility of $5750\pm100\,\mathrm{cm}^2/\mathrm{Vs}$ for device B, respectively, both at room temperature. The channel is situated 30 nm below the surface. The dielectric constant of the AlGaAs barrier is $\epsilon_r \approx 13$. Fig. 1 (b) shows the geometrical layout of sample A. The ohmic source and drain contacts of device A (B) are separated by $2.4\,\mu$m ($3.8\,\mu$m), thereof $L = 1.2\,\mu$m ($1.2\,\mu$m) are gated, i.e. the rectifying part of the structure, whereas $L_{acc} = 0.6\,\mu$m ($1.3\,\mu$m) remain ungated due to processing limitations causing an access impedance. The channel is $W = 15\,\mu$m ($30\,\mu$m) wide. The gate is deposited on top of the source terminal, being separated by a dielectric SiN spacer of 100 nm thickness. This ensures strong AC coupling of source and gate, required for efficient operation of the FET [18], [19]. The active element is attached to a self-complementary logarithmic spiral antenna. Only its inner part is shown. Fig. 1 (c) shows the package of a device integrated with a hyper-hemispherical silicon lens. Each device is mounted at the center of the lens inside the housing.

III. Theoretical Description

THz radiation fed into the channel of a FET is rectified along the penetration direction into the channel if the THz frequency is above the cut-off frequency of the transistor for amplification (f_T, f_{max}). Since the THz radiation is rectified, it penetrates only a certain length, the effective rectification length, L_{eff}, into the channel.

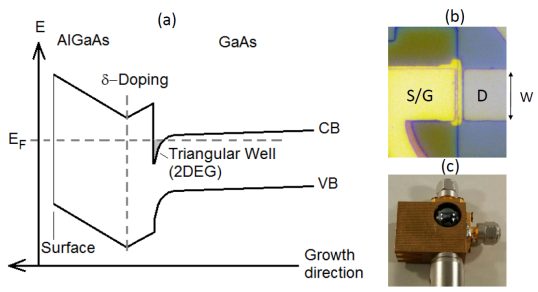

Fig. 1. (a) HEMT band structure of the FET. (b) Micrograph of the fabricated device A. (c) Silicon-lens integrated housing

In short channels that are shorter than the effective rectification length ($L_{\mathrm{eff}} > L$) the gated area forms a (lossy) cavity for the THz radiation with several round trips [20], where cavity resonances may be expected. In this paper, however, we are interested in broadband THz detection with a bandwidth of several octaves. Therefore, only long channels ($L_{\mathrm{eff}} \ll L$) are used where no resonances occur, even if the device is operated in the plasma-resonant region ($\omega\tau \geq 1$). In the following, we revise and derive the lumped element values for the equivalent circuit in FET rectifiers. The theoretical model is largely based on the derivations for the long channel limit for the resonant and non-resonant case [10], [14], [21]. The antenna-coupled field effect transistor can be modeled by four circuit elements as illustrated in Fig. 2: (I) the antenna, represented by its radiation impedance, Z_A, and a bias source in series, (II) the gate-drain capacitance, C_{GD}, which shorts the power transmission into the channel at high frequencies, (III) the access resistance due to ungated parts of the transistor and other unwanted contributions, and (IV) the active part, which can be modeled as a transmission line [10]. The high electron mobility transistors (HEMT) presented in this work feature a strong AC coupling of gate and source by AC shorting the gate and source with the capacitor C_{Sh}. In the following, the circuit elements will be derived. *The radiation resistance* couples the received power of

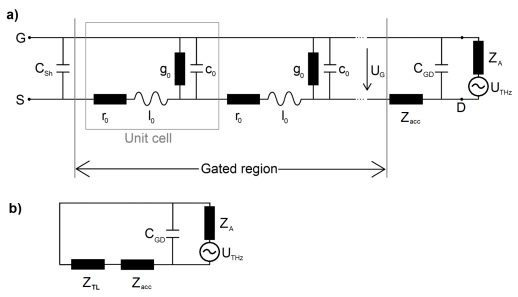

Fig. 2. (a) Detailed equivalent circuit of the FET. (b) Lumped element representation.

$$P_{\text{THz}} = \frac{1}{2R_A} U_{\text{THz}}^2 \tag{1}$$

to the circuit. We implement broadband logarithmic-periodic spiral antennas with a radiation resistance of around $72\,\Omega$ between $50\,\text{GHz}$ and $0.7\,\text{THz}$. At higher frequencies, the finite size of the FET and its electrodes at the center of the spiral modify the radiation resistance. Therefore, Z_A as well as the polarization is determined by simulations using CST microwave studio for the whole investigated frequency range. While the polarization is circular for frequencies below ~ 1 THz it becomes elliptic, reaching an ellipticity (ratio between the polarization half axes) of 3 at $1.5\,\text{THz}$ for device A and at $1.25\,\text{THz}$ for device B. For much higher frequencies the polarization becomes linear and the radiation resistance is determined only by the geometry of the active element.

The gate-drain capacitance requires also simulations performed in CST microwave studio. For the electrode structure depicted in Fig. 1 the capacitance is $C_{GD} = 3.09\,\text{pF}$ for device A ($C_{GD} = 3.66\,\text{pF}$ for device B).

The access impedance is dominated by the ungated parts of the channel. It follows from a simple RF Drude model with the general conductance

$$\sigma^{(2D)}(\omega) = \frac{\sigma_{DC}^{(2D)}}{1 + j\omega\tau}, \tag{2}$$

with $\sigma_{DC}^{(2D)} = en^{(2D)}\mu_{DC}$ the DC (sheet) conductivity, e the elementary charge, $n^{(2D)}$ the sheet charge density of the 2DEG, and $\mu_{DC} = e\tau/m^*$ the DC carrier mobility. τ is the momentum scattering time and m^* is the effective mass of the carrier, in this case, the electron effective mass of $m^* = 0.067m_0$ of electrons in GaAs. The impedance of the ungated part of the channel is thus

$$Z_{acc} = \frac{1}{\sigma^{(2D)}(\omega)} \cdot \frac{L_{acc}}{W} = \frac{1}{\sigma_{DC}^{(2D)} W} L_{acc} + \frac{j\omega\tau}{\sigma_{DC}^{(2D)} W} L_{acc}, \tag{3}$$

where W is the width and L_{acc} is the length of the ungated part of the channel. An alternative way to express the access resistance from Eq. 3 is

$$Z_{acc} = r_0^{acc} L_{acc} + j\omega l_0^{acc} L_{acc}, \tag{4}$$

where $r_0^{acc} = (\sigma_{DC}^{(2D)} W)^{-1}$ is the resistance per unit length and $l_0^{acc} = \tau r_0^{acc}$ is the inductance per unit length. The transistors used in this work feature a 2DEG sheet resistance of $r_0^{(2D)} = 2.3\,k\Omega/\square$ for device A ($r_0^{(2D)} = 1.5\,k\Omega/\square$ for device B).

The impedance of the rectifying element, Z_{TL} can be derived from a transmission line model, [10], [14], [21]

$$\frac{\partial}{\partial x} U_{\text{THz}}(x) = -(r_0 + j\omega l_0) I_{\text{THz}}(x) \tag{5}$$

$$\frac{\partial}{\partial x} I_{\text{THz}}(x) = -(g_0 + j\omega c_0) U_{\text{THz}}(x), \tag{6}$$

where $c_0 = \epsilon_0\epsilon_r W/d$ is the gate-channel capacitance per unit length with d the channel depth below the surface, g_0 is the gate-channel conductance per unit length of a lossy gate which is typically so small that it can be neglected ($g_0 = 0$ in the following), and r_0 and l_0 are the channel's resistance and inductance per unit length, mathematically identical to those derived for the access impedance, r_0^{acc} and l_0^{acc} in Eq. 4. In practice, the gate metal modifies the surface charge of the remotely doped high electron mobility transistor (HEMT). Therefore, the charge density $n^{(2D)}$ in the gated and ungated parts of the channel may differ. However, the threshold bias obtained from DC measurements is in good agreement (deviation in $U_{th} \leq 0.1\,\text{V}$) with the theoretically expected value from the Hall measurement for both wafers. The general solution of Eq. 5 and Eq. 6 is $U_{\text{THz}}(x) = U_0 \exp(-\gamma x)$ where U_0 is the THz bias at the beginning of the gate and the complex wave vector

$$\begin{aligned} \gamma &= \pm\sqrt{(r_0 + j\omega l_0)(g_0 + j\omega c_0)} \\ &= \pm\sqrt{(r_0[1 + j\omega\tau])(j\omega c_0)} \\ &= \frac{1}{L_{\text{eff}}} + jk \end{aligned} \tag{7}$$

The sign of γ depends on the boundary conditions and has to be chosen such that the wave is attenuated along the propagation direction for operation above amplification cut-off frequencies. L_{eff} is the effective penetration depth of the THz radiation into the channel, while k is the wave vector of the plasma wave, which is related to the group velocity by $v_g = \partial\omega/\partial k$ (phase velocity $v_{ph} = \omega/k$). The effective penetration depth is

$$L_{\text{eff}}(\omega) = \frac{1}{\sqrt{\left(\sqrt{1 + (\omega\tau)^2} - \omega\tau\right)}} L_{\text{eff}}^{nr}(\omega), \tag{8}$$

where $L_{\text{eff}}^{nr} = \sqrt{2 \cdot (\omega r_0 c_0)^{-1}}$ is the effective length for a non-lossy gate ($g_0 = 0$) for non-resonant operation ($l_0 = 0$) that was derived in [10]. While L_{eff} decreases with increasing frequency in the non-resonant case , the resonant effective length approaches a constant value,

$$L_{\text{eff}}^{\infty} = \lim_{\omega\to\infty} L_{\text{eff}}(\omega) = 2\sqrt{\frac{\tau}{r_0 c_0}}. \tag{9}$$

Expressing L_{eff}^{∞} by materials parameters and geometry yields

$$L_{\text{eff}}^{\infty} = 2e\tau\sqrt{\frac{n^{(2D)}d}{m^*\epsilon_0\epsilon_r}} = 2\mu_{DC}\sqrt{\frac{m^* n^{(2D)} d}{\epsilon_0\epsilon_r}}. \tag{10}$$

Channel lengths of about 2 to 3 L_{eff} suffice to reach the long channel regime. Much longer channels increase the DC resistance and therefore cause additional Johnson-Nyquist noise, deteriorating the noise floor of the receiver. III-V HEMTs used in this paper have an effective rectification length $L_{\text{eff}}^{\infty} \approx 310\,\text{nm}$ in the limit of high frequencies for device A and $L_{\text{eff}}^{\infty} \approx 370\,\text{nm}$ for device B. Therefore, channel lengths in the range of $1\,\mu$m that can be achieved with UV contact lithography as used in this paper, suffice for efficient THz operation, even at highest frequencies. In contrast, silicon FETs offer much lower mobilities in the range of $110\,\text{cm}^2$/Vs [22] with similar effective barrier heights, d/ϵ_r, and carrier concentrations in the range of 1 to $10 \cdot 10^{11}\,/(cm)^2$, leading to minimum rectification lengths of only 5 to 16 nm. Therefore, efficient Si FETs for frequencies in the plasma-resonant range require high-end processing in the range of 65 nm technology or better while III-V FETs are much less demanding.

The impedance of the gated part of the channel, where the THz signal is rectified is

$$Z_{\text{TL}} = \sqrt{\frac{r_0 + j\omega l_0}{g_0 + j\omega c_0}} = \sqrt{\frac{r_0(1 + j\omega\tau)}{j\omega c_0}}. \qquad (11)$$

It should be noted that the inductive part of the channel can be neglected if $\omega\tau \ll 1$ which is termed the non-resonant operation range [10] while for $\omega\tau \geq 1$, the channel features both inductive and capacitive elements, causing a plasma wave to spread in the channel. This regime is called the plasma-resonant range. Transistors used in this paper feature a transition frequency from non-resonant to resonant of $\omega\tau = 1$ for approx. 0.71 THz. The investigated frequency range from 100 GHz to 11.8 THz therefore covers both non-resonant and resonant regimes.

The current responsivity of the FET is given by

$$\mathcal{R}_I = \mathcal{R}_I^{id} f \eta_{Op} \eta_{El}, \qquad (12)$$

where $\mathcal{R}_I^{id}$ is the ideal (low frequency) responsivity, η_{Op} considers optical losses by mismatch of the THz spot size and the antenna size as well as polarization issues and η_{El} the roll-off due to bias losses within the circuit. The plasmonic efficiency factor f [22] for the case of an AC-shorted source-gate is

$$|f| = 1 + \frac{2\omega\tau}{\sqrt{1 + (\omega\tau)^2}} \frac{\sinh^2 L/L_{\text{eff}} - \sin^2 Lk}{\cosh^2 L/L_{\text{eff}} - \cos^2 Lk}, \qquad (13)$$

with the complex wave vector $\gamma = \frac{1}{L_{\text{eff}}} + jk$ from Eq. 7. The plasmonic efficiency $|f|$ shows a smooth transition from 1 to 3 for the investigated frequency range. The transistors used for this study operate in the long gate regime, thus there are no oscillations in the plasmonic efficiency f.

The ideal responsivity in the low frequency limit is

$$\mathcal{R}_I^{id} = \frac{\Delta I_d}{P_{\text{THz}}} = \frac{\mu c_0 R_A}{L_{\text{eff}}}. \qquad (14)$$

For $L_{\text{eff}}^{\infty} = 310$ nm, a radiation resistance of 72 Ω and a mobility of 5850± 150 cm^2/Vs, the ideal current responsivity becomes $\mathcal{R}_I^{id} = 7.8$ A/W and is similar for both transistors. Since the rectified signal is proportional to the square of the bias delivered to the device impedance, Z_{TL}, the roll-off is given by

$$\eta_{El} = \left| \frac{U_{\text{TL}}}{U_{\text{THz}}} \right|^2, \qquad (15)$$

where U_{TL} is the bias that drops at the impedance Z_{TL} of the active element in Eq. 11 and $U_{\text{THz}} = \sqrt{2 R_A P_{\text{THz}}}$ is the input THz bias to the circuit from the antenna. η_{El} can be calculated from the equivalent circuit model in Fig. 2 (b), equations Eq. 3, Eq. 11, the simulated capacitance C_{GD} and antenna impedance Z_A.

IV. Experimental Results

The FETs were characterized with three different setups. For frequencies between 100 GHz and 1.6 THz, a 1550 nm operated pin-diode photomixer (Toptica Photonics, Fraunhofer Heinrich Hertz Institute) is used as continuous wave (CW) source, modulated at 12 kHz for lock-in detection. The reference power of the pin-diode is measured with a Golay cell that is calibrated to a Thomas Keating power meter. The THz signal from the p-i-n diode is guided and focused on the FET using two parabolic mirrows and two TPX lenses. At 3.8 THz, the data are extended using a QCL, bias-modulated at 1.11 kHz. The fairly elliptical beam is first collimated by a TPX lens with $f = 50$ mm and then focused on the FET using another TPX lens of the same kind. The reference power is determined using a 28.3 mm^2 pyroelectric detector. While the active area of the pyroelectric detector is larger than the elliptic spot and therefore captures all emitted power from the QCL, the coupling losses to the much smaller receiving area of the FET due to beam ellipticity is estimated to a factor of 1.75. In both experiments, a transconductance amplifier (TEM Messtechnik, PDA-S) at a gain of 10^6 V/A is used prior to lock-in detection. The data are completed by two measurements at 2.0 THz and 11.8 THz at the free electron laser FELBE at the Helmholtz-Zentrum Dresden-Rossendorf. The FEL was operated in the quasi-CW mode with single THz pulses, the device was operated in the unsaturated, linear regime. The signal was recorded using a 30 GHz oscilloscope. The reference power was measured with a thermal power meter. In all cases, the sources feature linear polarization. First the devices are characterized with respect to the best optimum operation point. The optimum bias for lowest

NEP is a compromise between high responsivity, being higher closer to threshold, and low thermal noise, being lower at positive gate biases due to a smaller device resistance. The optimum operation point is usually found in the vicinity of the point of highest transconductance. Fig. 3 shows that the transconductance of device A is at maximum close to $U_{GS} = 0\,\mathrm{V}$, qualifying the transistor for zero-bias operation. THz measurements below 1 THz confirm an optimum gate bias for lowest NEP at $U_{GS} = 0\,\mathrm{V}$, where the responsivity is largest.

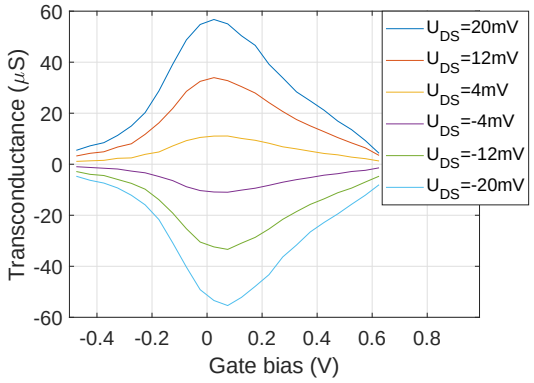

Fig. 3. DC transconductance of sample A, showing a pronounced extremum close to 0 V gate bias, qualifying the transistor for zero-bias operation.

Fig. 4 shows the THz responsivity for both devices under zero-bias (sample A) and biased operation (sample B) in comparison to the theoretical model from Eq. 12. The experimental data are corrected for 30% reflection of the silicon lens and the frequency dependent polarization mismatch. There is very good agreement over the whole examined frequency range covering more than two decades for both the CW and pulsed THz measurements except for the antenna resonance in the simulations around 3.7 THz which is not observed in the measurements.

To the knowledge of the authors, this is the largest frequency range where measurements on individual FETs proof the validity of the equivalent circuit model presented in Fig. 2. The responsivity decreases only gently up to about 600 GHz with a corresponding NEP value of $250\,\mathrm{pW}/\sqrt{\mathrm{Hz}}$, following approximately an f^{-1} decrease as suggested by the model for non-resonant operation [10] and then decreases roughly with f^{-4} up to the highest measured frequency of 11.8 THz, mainly due to the low pass filter of 2^{nd} order caused by the access impedance and the gate-drain capacitance, C_{GD}. With a conjugate-matched resonant antenna, the responsivity is expected to be enhanced by an order of magnitude at 2 THz, as indicated by the star in the figure.

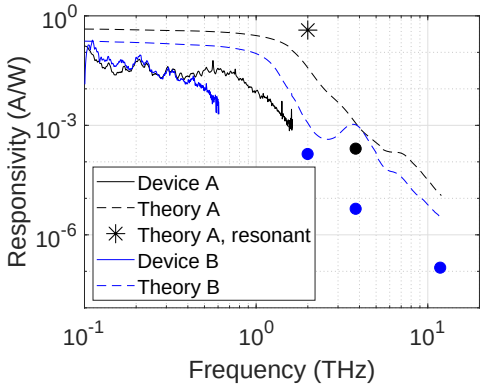

Fig. 4. Measured and calculated responsivity of device A and B. The peak in the theoretical responsivity for device B between 3 and 4 THz arises from a resonance in the antenna simulations which is not observed in the experiment. The measurements are referenced by the total (peak) power of the respective sources and are only corrected for the frequency dependent polarization mismatch and the reflection of the silicon lens. With a resonant antenna the responsivity is expected to increase by an order of magnitude at 2 THz (star).

V. Conclusion and Outlook

We have demonstrated that UV contact-lithographically processed III-V high mobility transistors can reach noise equivalent powers with a single ultra-broadband antenna only one order of magnitude above CMOS fabricated silicon-based FETs using 65 nm technology and narrow-band, resonant designs. The devices are optimized for zero-bias operation, simplifying experimental requirements and thus being an alternative to Schottky diodes. We showed the versatility of the transistors operating with low power CW THz radiation from a table-top source as well as with ultra-short high power pulses from a free electron laser.

Whilst the devices used in this work still possess separate gate and source electrodes in order to be able to measure the transconductance and to proof efficient operation at zero gate bias, future devices can be processed with a short between gate and source terminal. We further have demonstrated good agreement of the measured device responsivity with a theoretical model over the extreme frequency range of 100 GHz to 11.8 THz, proofing the validity of the model. In the resonant regime, the responsivity rolls off with f^{-4} due to a low pass of 2^{nd} order caused by the access impedance and the gate-drain capacitance. The model now allows to derive improved designs for future devices with optimized geometrical parameters.

Acknowledgment

We are grateful to P. Michel and the FELBE team for their dedicated support. The authors would like to

thank D. Čibiraitė, A. Lisauskas and H. Roskos from Johann Wolfgang Goethe-Universität, Frankfurt(Main), Germany for help with the calibration of the Golay cell and the CST AG for providing the CST Studio Suite. This work was supported by the Deutsche Forschungsgemeinschaft, Project PR1413/2-1 (LA-FET).

REFERENCES

[1] D. Glaab, S. Boppel, A. Lisauskas, U. Pfeiffer, E. Öjefors, and H. G. Roskos, "Terahertz heterodyne detection with silicon field-effect transistors," *Applied Physics Letters*, vol. 96, no. 4, p. 042106, jan 2010.

[2] M. Hoefle, K. Haehnsen, I. Oprea, O. Cojocari, A. Penirschke, and R. Jakoby, "Compact and Sensitive Millimetre Wave Detectors Based on Low Barrier Schottky Diodes on Impedance Matched Planar Antennas," *Journal of Infrared, Millimeter, and Terahertz Waves*, vol. 35, no. 11, pp. 891–908, nov 2014.

[3] J. L. Hesler, T. W. Crowe, and V. Diodes, "Responsivity and Noise Measurements of Zero-Bias Schottky Diode Detectors," in *Proc. 18th International Symposium on Space Terahertz Technology*, mar 2007, pp. 89–92.

[4] C. Sydlo, O. Cojocari, D. Schoenherr, T. Goebel, S. Jatta, H. L. Hartnagel, and P. Meissner, "Ultrawideband THz detector based on a zero- bias Schottky diode," in *Proc. 19th International Symposium on Space Terahertz Technology*, apr 2008, p. 226.

[5] E. R. Brown, A. C. Young, J. E. Bjarnason, J. D. Zimmerman, A. C. Gossard, and H. Kazemi, "Millimeter and sub-millimeter wave performance of an ErAs:InAlGaAs Schottky diode coupled to a single-turn square spiral," *International Journal of High Speed Electronics and Systems*, vol. 17, no. 02, pp. 383–394, jun 2007.

[6] W. Knap, F. Teppe, N. Dyakonova, D. Coquillat, and J. Łusakowski, "Plasma wave oscillations in nanometer field effect transistors for terahertz detection and emission," *Journal of Physics: Condensed Matter*, vol. 20, no. 38, p. 384205, sep 2008.

[7] W. Knap, V. Kachorovskii, Y. Deng, S. Rumyantsev, J.-Q. Lü, R. Gaska, M. S. Shur, G. Simin, X. Hu, M. A. Khan, C. A. Saylor, and L. C. Brunel, "Nonresonant detection of terahertz radiation in field effect transistors," *Journal of Applied Physics*, vol. 91, no. 11, p. 9346, may 2002.

[8] S. Regensburger, M. Mittendorff, S. Winnerl, H. Lu, A. C. Gossard, and S. Preu, "Broadband THz detection from 0.1 to 22 THz with large area field-effect transistors," *Optics express*, vol. 23, no. 16, pp. 20732–20742, aug 2015.

[9] K. Ikamas, A. Lisauskas, S. Boppel, Q. Hu, and H. G. Roskos, "Efficient Detection of 3 THz Radiation from Quantum Cascade Laser Using Silicon CMOS Detectors," *Journal of Infrared, Millimeter, and Terahertz Waves*, vol. 38, no. 10, pp. 1183–1188, oct 2017.

[10] S. Preu, S. Kim, R. Verma, P. G. Burke, M. S. Sherwin, and A. C. Gossard, "An improved model for non-resonant terahertz detection in field-effect transistors," *Journal of Applied Physics*, vol. 111, no. 2, p. 024502, jan 2012.

[11] D. Veksler, F. Teppe, A. Dmitriev, V. Kachorovskii, W. Knap, and M. Shur, "Detection of terahertz radiation in gated two-dimensional structures governed by dc current," *Physical Review B*, vol. 73, no. 12, p. 125328, mar 2006.

[12] J. Grzyb and U. Pfeiffer, "THz Direct Detector and Heterodyne Receiver Arrays in Silicon Nanoscale Technologies," *Journal of Infrared, Millimeter, and Terahertz Waves*, vol. 36, no. 10, pp. 998–1032, oct 2015.

[13] M. Bauer, R. Venckevičius, I. Kašalynas, S. Boppel, M. Mundt, L. Minkevičius, A. Lisauskas, G. Valušis, V. Krozer, and H. G. Roskos, "Antenna-coupled field-effect transistors for multi-spectral terahertz imaging up to 4.25 THz," *Optics express*, vol. 22, no. 16, p. 19235, aug 2014.

[14] S. Boppel, A. Lisauskas, and H. G. Roskos, "Terahertz array imagers: Towards the implementation of terahertz cameras with plasma-wave-based silicon MOSFET detectors," in *Handbook of Terahertz Technology for Imaging, Sensing and Communications*. Elsevier, 2013, pp. 231–271.

[15] U. R. Pfeiffer and E. Öjefors, "A 600-GHz CMOS focal-plane array for terahertz imaging applications," *Proc. 34th European Solid-State Circuits Conference*, sep 2008, pp. 110–113.

[16] I. Khmyrova and Y. Seijyou, "Analysis of plasma oscillations in high-electron mobility transistorlike structures: Distributed circuit approach," *Applied Physics Letters*, vol. 91, no. 14, p. 143515, oct 2007.

[17] C. Deutsch, M. A. Kainz, M. Krall, M. Brandstetter, D. Bachmann, S. Schönhuber, H. Detz, T. Zederbauer, D. MacFarland, A. M. Andrews, W. Schrenk, M. Beck, K. Ohtani, J. Faist, G. Strasser, and K. Unterrainer, "High-Power Growth-Robust InGaAs/InAlAs Terahertz Quantum Cascade Lasers," *ACS Photonics*, vol. 4, no. 4, pp. 957–962, apr 2017.

[18] S. Boppel, M. Ragauskas, A. Hajo, M. Bauer, A. Lisauskas, S. Chevtchenko, A. Ramer, I. Kasalynas, G. Valusis, H.-J. Wurfl, W. Heinrich, G. Trankle, V. Krozer, and H. G. Roskos, "0.25-um GaN TeraFETs Optimized as THz Power Detectors and Intensity-Gradient Sensors," *IEEE Transactions on Terahertz Science and Technology*, vol. 6, no. 2, p. 348, mar 2016.

[19] S. Regensburger, S. Winnerl, J. M. Klopf, H. Lu, A. C. Gossard, and S. Preu, "Investigation of parasitic coupling of THz radiation to a large area field-effect transistor," in *Proc. 2017 42nd International Conference on Infrared, Millimeter, and Terahertz Waves (IRMMW-THz)*, aug 2017.

[20] V. Ryzhii, A. Satou, W. Knap, and M. S. Shur, "Plasma oscillations in high-electron-mobility transistors with recessed gate," *Journal of Applied Physics*, vol. 99, no. 8, p. 084507, apr 2006.

[21] M. A. Andersson and J. Stake, "An Accurate Empirical Model Based on Volterra Series for FET Power Detectors," *IEEE Transactions on Microwave Theory and Techniques*, vol. 64, no. 5, pp. 1431–1441, may 2016.

[22] S. Boppel, A. Lisauskas, M. Mundt, D. Seliuta, L. Minkevicius, I. Kasalynas, G. Valusis, M. Mittendorff, S. Winnerl, V. Krozer, and H. G. Roskos, "CMOS Integrated Antenna-Coupled Field-Effect Transistors for the Detection of Radiation From 0.2 to 4.3 THz," *IEEE Transactions on Microwave Theory and Techniques*, vol. 60, no. 12, pp. 3834–3843, dec 2012.

Stefan Regensburger received the B.Sc. and M.Sc. degree in Physics from the Friedrich-Alexander Universität Erlangen-Nürnberg, Germany in 2011 and 2013, respectively. Since 2014 he is a Ph.D. student in the Terahertz Systems Technology group at the Department of Electrical Engineering and Information Technology, Technische Universität Darmstadt, Germany.

His research interests focus on field effect transistor rectifiers and THz spectroscopy of conductive thin films.

Amlan kusum Mukherjee received the B.Tech. degree from National Institute of Technology, Durgapur, India in 2013 and the M.Sc. degree from Technische Universität Darmstadt, Germany in 2018. He is currently working towards the Ph.D. degree in the Terahertz Systems Technology group at TU Darmstadt. His research interests include transistor based antenna-coupled Terahertz detectors and Terahertz waveguides.

Sebastian Schönhuber studied technical physics at the TU Wien and received his M.Sc. in 2015. Since 2015 he is a PhD student in the Terahertz Group at the Photonics Institute at the Faculty of Electrical Engineering and Information Technology, TU Wien, Austria. His research activities are focused on cavity concepts for Quantum Cascade Lasers based on Random Structures. He is secretary of the OSA Vienna student chapter and member of the ÖPG.

Martin A. Kainz studied technical physics at the TU Wien, Austria. He did his master's thesis in collaboration at the Institute for Ion Physics and Applied Physics, Universität Innsbruck, Austria and received his M.Sc. degree in 2015. Since 2015 he is a PhD student in the Terahertz Group at the Faculty of Electrical Engineering and Information Technology, TU Wien, Austria. His research interests include material aspects for high temperature terahertz quantum cascade lasers.

Stephan Winnerl received the Diploma degree and Ph.D. degree from the University of Regensburg, Regensburg, Germany, in 1996 and 1999, respectively.
He spent two and a half years as a Post-Doctoral Member at the Forschungszentrum Jülich. Since 2002, he has been with the Helmholtz-Zentrum Dresden-Rossendorf (HZDR, formerly Forschungszentrum Dresden-Rossendorf), Dresden, Germany, and was appointed as HZDR Research Fellow in 2014. He has authored and coauthored more than 175 peer-reviewed publications. His research interest is on ultrafast and nonlinear spectroscopy of semiconductor quantum structures and 2D materials, in particular in the THz frequency range. Furthermore, he develops emitters and fast detectors for THz radiation.
Dr. Winnerl is a member of the German Physical Society.

J. Michael Klopf received his B.S. in physics from Louisiana State University in 1993 and his Ph.D. in engineering physics from the University of Virginia in 2005. Before graduate school, he worked as a Research Associate at the CAMD synchrotron facility. In 2005, he began work in the Free Electron Laser Division at the Thomas Jefferson National Accelerator Facility, first as a postdoc, then as a staff scientist. Since 2015, he has been the FEL Beamline Scientist in the ELBE Center for High-Power Radiation Sources at HZDR in Dresden, Germany. He has authored and coauthored more than 50 journal and conference publications and holds one U.S. patent. His research interests are focused on laser driven ultrafast dynamics in materials and applications related to FEL and accelerator physics. He is a member of the American Physical Society and the German Physical Society.

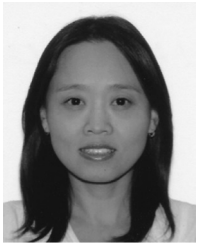

Hong Lu received the B.S. degree in chemistry from the University of Science and Technology of China, Hefei, China, and the Ph.D. degree in chemistry from the City University of New York, New York, NY, USA, in 2007, where she focused on intersubband transitions of wide-bandgap II-VI semiconductors grown by molecular beam epitaxy (MBE).
After working as a project scientist at the Materials Department, University of California, Santa Barbara, CA, USA for 8 years, Hong joined Nanjing University and she is currently a Professor with the Department of Materials Science and Engineering, College of Engineering and Applied Sciences at Nanjing University. She has co-authored more than 100 papers in refereed journals. Her current research interests include using and developing MBE growth techniques for synthesis of novel materials and material structures, and characterization and processing for fundamental understanding and device applications, especially heterostructures formed by semiconductors, metals and semimetals, and their applications in optoelectronics, thermal management and tetrahertz-based technology.

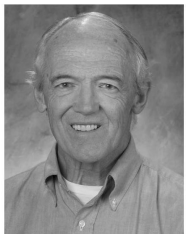

Arthur C. Gossard (LF'12) is currently a Professor of Materials and Electrical and Computer Engineering with the University of California, Santa Barbara, CA, USA.
His current research interests include molecular beam epitaxy, the growth of quantum wells and super lattices, and their applications to highperformance electrical and optical devices. Prof. Gossard is a fellow of the American Physical Society and the American Association for the Advancement of Science, Washington, DC, USA.
He is a member of the National Academy of Engineering and the National Academy of Sciences.

Karl Unterrainer received the MS degree in Physics from the University of Innsbruck in 1986, and his Ph.D. degree in 1989 for his work on stimulated far infrared emission. Subsequently, he worked as a research assistant at the Institute for Experimental Physics and developed a far infrared tunable cyclotron resonance laser. In 1992 he became assistant professor at the Technical University Vienna. In 1994 and 1995 he worked as a visiting researcher at the Quantum Institute, University of California, Santa Barbara. He used nonlinear THz spectroscopy to study intersubband relaxation rates and observed the inverse Bloch oscillator effect. From 1997 till 2003 he was associate professor at the Technical University Vienna. Since 2004 he his full professor at the Photonics Institute, Technical University Vienna. He has been the director of the Center of Micro&Nanostructures and of the Photonics Institute, and served as dean of the Faculty of Electrical Engineering and Information Technology, TU Wien. His main research areas are nano photonics, semiconductor nanostructures, time-resolved THz spectroscopy, and the development of THz devices. He is author or coauthor of more than 300 scientific articles.

Sascha Preu received the Diploma degree (2005) and the Ph.D. degree in Physics (summa cum laude) from the Friedrich-Alexander Universität Erlangen-Nürnberg, in 2009. From 2004-2010 he was working at the Max Planck Institute for the Science of Light, Erlangen, Germany. 2010-2011 he worked at the Materials and Physics Department, University of Santa Barbara, California. From 2011-2014 he was at the Chair of Applied Physics, Universität Erlangen-Nürnberg. Currently he is J.Professor at the Department of Electrical Engineering and Information Technology, Technische Universität Darmstadt, Germany, leading the Terahertz Systems Technology group. He authored and coauthored more than 70 journal articles or conference contributions. His research interests focus on the development of semiconductor-based THz sources and detectors, including photomixers, photoconductors and field effect transistor rectifiers. He also works on applications of THz radiation, in particular the characterization of novel THz components and materials, including graphene.